Alloying effects on the electronic structure of chromium

1996 J. Phys.: Condens. Matter 8 3619

(http://iopscience.iop.org/0953-8984/8/20/008)

J. Phys.: Condens. Matter **8** (1996) 3619–3634. Printed in the UK

Alloying effects on the electronic structure of chromium

Yoshihisa Matsumoto†, Masahiko Morinaga‡, Tomonori Nambu§ and Takashi Sakaki‖

† Department of Computer and Control Engineering, Oita National College of Technology, Maki, Oita 870-01, Japan

‡ Department of Materials Science and Engineering, School of Engineering, Nagoya University, Furo-cho, Chikusa-ku, Nagoya, Aichi 464-01, Japan

§ Department of Materials Science and Engineering, Suzuka National College of Technology, Shirako-cho, Suzuka, Mie 510-02, Japan

‖ Chemical Laboratories, Tosoh Corporation Ltd, Kaisei-cho, Shin-nanyo, Yamaguchi 746, Japan

Received 14 September 1995, in final form 19 January 1996

Abstract. Alloying effects on the electronic structure of Cr metal were investigated in order to obtain useful information for alloy design. The electronic structures were calculated by the DV–Xα molecular orbital method, and two alloying parameters were determined theoretically. One was the d-orbital energy level Md and the other was the bond order Bo for various alloying elements M in Cr. By using these parameters, alloying behaviour was elucidated successfully. For example, the solidus temperature of binary Cr–M alloys showed a positive correlation with the bond order Bo. Also, the solubility limits of alloying elements in the Cr solid solution at 873 K were associated with Md and Bo. Furthermore, the appearance of intermetallic compounds, e.g. the σ-phase and the Laves phase in the Cr binary system, was predictable with these alloying parameters. The present results were shown to be useful as a guide for designing high-performance chromium-based alloys.

1. Introduction

Chromium and its alloys exhibit an excellent combination of low density, high creep strength and good oxidation resistance at high temperatures [1]. There have been numerous investigations on this alloy system because of the high potential for applications to structural materials, device materials, or some parts of machines. For example, magnetic and thermodynamic properties have been studied extensively for pure Cr [2–8]. However, there still remains an important problem for practical use, i.e. the very poor ductility of pure Cr at room temperature. Many previous investigations [9–12] have been concerned with this problem. In the 1960s, several alloying elements which could make Cr metal more ductile were found experimentally [13, 14], but still the improvement in the ductility by alloying was not satisfactory from the viewpoint of the practical use. The alloying effects on the ductility were not understood and yet were partially due to the relatively low purity of raw chromium metal, causing a large scattering in the mechanical data of Cr alloys.

Sigli and Sanchez [15] have attempted to estimate the energies for the ordering or the segregation of atoms in Cr binary alloys from the calculation of electronic structures. A commensurate-to-incommensurate transition of the spin-density wave has also been discussed for Cr–Mn and Cr–Fe alloys [16]. There is relatively good agreement between the electronic structures of pure Cr given by several band calculations [2, 17–21]. However,

0953-8984/96/203619+16$19.50

the calculations of electronic states involving some alloying elements [4, 15, 16, 22] are so limited that there are still many difficulties in understanding the alloying behaviour in Cr.

Recently, alloying effects on the electronic structures of some BCC metals (e.g. Ti, V, Fe, Zr, Nb and Mo) have been estimated using the discrete variational (DV)–Xα method [23–27]. The characteristics of these BCC alloys are well represented by alloying parameters determined from the calculations [28–30]. For instance, binary phase diagrams for Ti-, Nb- and Mo-based alloys could be classified accurately into several types using such parameters [23, 27]. Therefore, this approach is worth applying to BCC Cr-based alloys, in order to obtain useful information for alloy design.

The purpose of this study is to calculate the electronic structures of BCC Cr containing 3d, 4d and 5d transition elements by using the DV–Xα cluster method [31–34]. The alloying parameters such as the d-orbital energy level and the bond order between solute and solvent atoms were obtained for a variety of alloying transition elements in Cr. The solidus temperature and the solubility limit of binary Cr alloys were found to be predictable with the aid of these calculated alloying parameters. The trend of the appearance of some intermetallic compounds such as the σ-phase and the Laves phase in Cr alloys will also be discussed in terms of these theoretical alloying parameters.

2. DV–Xα cluster method and cluster model

The DV–Xα cluster method [31–34] is a molecular orbital method based on the Hartree–Fock–Slater approximation. In this method [35], the exchange–correlation between electrons includes the Slater local exchange–correlation potential V_{xc} which is given by

$$V_{xc} = -3\alpha \left[\frac{3}{8\pi} \rho(r) \right]^{1/3} \tag{1}$$

where $\rho(r)$ is the local electron density at position r. The parameter α is fixed at a constant value of 0.7, an empirically appropriate value [33]. The self-consistent charge approximation is used in this calculation. The matrix elements of the Hamiltonian and the overlap integrals are calculated by the weighted sum of integrant values at a large number of discrete sample points chosen randomly in real space, instead of employing the normal integration procedure. Therefore, no mathematical restriction is placed on the integration of these matrix elements. Also, in contrast with the SW–Xα method [36], a muffin-tin potential is not used in the DV–Xα method. The molecular orbitals are constructed by a linear combination of numerically generated atomic orbitals. For chromium, the atomic orbitals used were 1s–4p. For an alloying element M, they were 1s–*n*p ($n = 4$ for Ti, V, Mn, Fe, Co, Ni and Cu (3d transition elements); $n = 5$ for Zr, Nb, Mo, Tc, Ru, Rh, Pd and Ag (4d transition elements); $n = 6$ for Hf, Ta, W, Re, Os, Ir, Pt and Au (5d transition elements)).

The cluster model used in this calculation is shown in figure 1. This MCr_{14} cluster having the O_h symmetry consisted of a central alloying element M, the surrounding eight first-nearest-neighbour chromium atoms ($Cr^{(1)}$) and the six second-nearest-neighbour chromium atoms ($Cr^{(2)}$). The lattice parameter used was 0.288 46 nm, the same value as in the bulk.

In this calculation, lattice relaxation was not taken into account on the $Cr^{(1)}$ and $Cr^{(2)}$ atomic positions neighbouring an alloying element, because there are no experimental data at the moment. The total energy calculation may be used for this problem but, as the elastic interaction is a long-range interaction, accurate estimation of the elastic energy is probably difficult even when using a very large size of the cluster model. Instead, the present

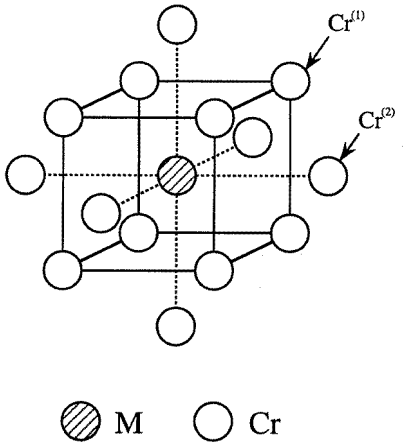

Figure 1. Cluster model of MCr_{14} (M = 3d, 4d and 5d transition elements) employed in the calculation. $Cr^{(1)}$ and $Cr^{(2)}$ are the first- and the second-nearest-neighbour atoms, respectively, from M.

calculation was performed, aiming to examine the general trend of the alloying behaviour of the elements with Cr. For this purpose any calculation involving large ambiguities in the mode of lattice relaxation was rather unsuitable. In addition, one may suppose that the cluster size shown in figure 1 is small. However, this is not the case, since the second-nearest-neighbour atomic interaction is not larger in Cr than in other BCC metals [24]. The present cluster is indeed empirically suitable for obtaining the alloying effect on the electronic structure in a concrete way [27–30].

For characterization of the electronic structure and the atomic bonding in Cr metal it is useful to investigate the energy level structure, the spatial charge distribution in a cluster, the ionicity and the bond order between atoms. Here, the spatial charge distribution was convenient to determine the redistribution of the valence electrons in Cr by alloying. The ionicity of elements and the bond order Bo were calculated following the Mulliken [37] population analysis. The former is a measure of charge transfer between atoms and the latter is a measure of the covalent bond strength between atoms. The energy distribution of the overlap populations between d electrons was also calculated in order to show how the d–d covalent interaction was modified by alloying.

The orbital population is convenient for defining the number of electrons occupying a given atomic orbital and, by summing them, the effective charge on the atom (the partial ionicity) can be estimated. The overlap population $Q_{\nu\nu'}$ of electrons between two atoms ν and ν' is defined as

$$Q_{\nu\nu'} = \sum_k \sum_{i,j} C_{ik}^{\nu} C_{jk}^{\nu'} \int \Psi_i^{\nu} \Psi_j^{*\nu'} \, \mathrm{d}V. \tag{2}$$

Here, Ψ_i^{ν} and $\Psi_j^{\nu'}$ are the wavefunctions of the i and j orbitals of atoms ν and ν', respectively. C_{ik}^{ν} and $C_{jk}^{\nu'}$ are the coefficients which show the magnitude of the linear combination of atomic orbitals in the kth molecular orbital. The sum over k runs only over the occupied orbitals. Here, $Q_{\nu\nu'}$ was called the bond order Bo and used as a measure of the strength of the covalent bonding.

In addition, the electron densities of states were calculated from the energy level structure by using the overlapping Gaussian distribution curves with a width of 0.2 eV and the centres located at each cluster energy level [38]. Furthermore, the d-orbital energy levels Md of alloying elements were obtained from the energy level structure of the alloy cluster shown in figure 1. According to our previous investigations [23, 24, 27], the Md value is known to be associated with the atomic radius and the electronegativity of element. With the aid of these calculated results, the alloying behaviour in BCC Cr was examined in detail in this study.

3. Results

3.1. Energy level structures of pure and alloyed Cr

The results for the energy level structure are shown in figure 2 for both pure Cr and alloyed Cr with 3d transition metals. In this figure, the Fermi energy level of pure Cr was set to be 0 eV and used as a reference. The Fermi energy level E_F for each cluster is indicated by an arrow in the figure. For pure Cr, the levels of $8e_g$ near -4 eV to $16t_{2g}$ near 2 eV originated mainly from the Cr 3d component and they formed a Cr 3d band at the Fermi energy level. Also, the levels labelled t_{2g} and e_g in figure 2 consisted mainly of the 3d orbitals of the central alloying transition element in the cluster with O_h symmetry. Those levels which have a largest fraction of the 3d component of the central element are indicated by broken lines in each level structure. For example, for the Ti-containing cluster there were 46% and 55% Ti 3d components in the $16t_{2g}$ and the $13e_g$ levels, respectively, both existing near 3 eV. As shown in the figure, the heights of these levels changed systematically with the order of elements in the periodic table. For the 4d and 5d alloying transition elements, such levels also appeared and varied in a similar way as the 3d transition elements.

3.2. d-orbital energy level Md

Table 1 is a list of the fractions of the 3d or 4d or 5d components in several t_{2g} and e_g levels, all existing near the broken levels shown in figure 2. For the Ti-containing cluster there were large fractions of the Ti 3d component only in the $16t_{2g}$ and the $13e_g$ levels as explained above. However, in some cases the fractions of the d component were split over several energy levels. For example, in the case of the Co addition, the fractions of the Co 3d component in the $16t_{2g}$, the $15t_{2g}$ and the $14t_{2g}$ levels were 10.0%, 5.6% and 8.6%, respectively. Therefore, the average t_{2g} level was calculated by taking the weighted average of the d components in the (14–16)t_{2g} levels for the 3d elements. Similarly, the averaging was taken using the (15–17)t_{2g} levels for the 4d elements and the (16–18)t_{2g} levels for the 5d elements. All these levels existed above the Fermi energy level E_F. In the same way, the average e_g level was calculated by using the (10–13)e_g levels for the 3d elements, the (11–14)e_g levels for the 4d elements and the (13–16)e_g levels for the 5d elements. The d-orbital energy level (Md) was then calculated by taking again the average of these calculated values for the t_{2g} and the e_g levels. The Md values for BCC Cr obtained in this way were drawn as full circles in figure 3(b) together with the results for BCC Mo and BCC Nb [27]. The Md curves changed with the order of elements in the periodic table. This change in the Md parameter with alloying elements for BCC Cr was similar to the result for BCC Mo and BCC Nb [27].

The Md parameter was related to the atomic radius of alloying element M [39], except for Cu, Pd, Ag, Pt and Au, as shown in figure 3(a). This is understood in terms of the

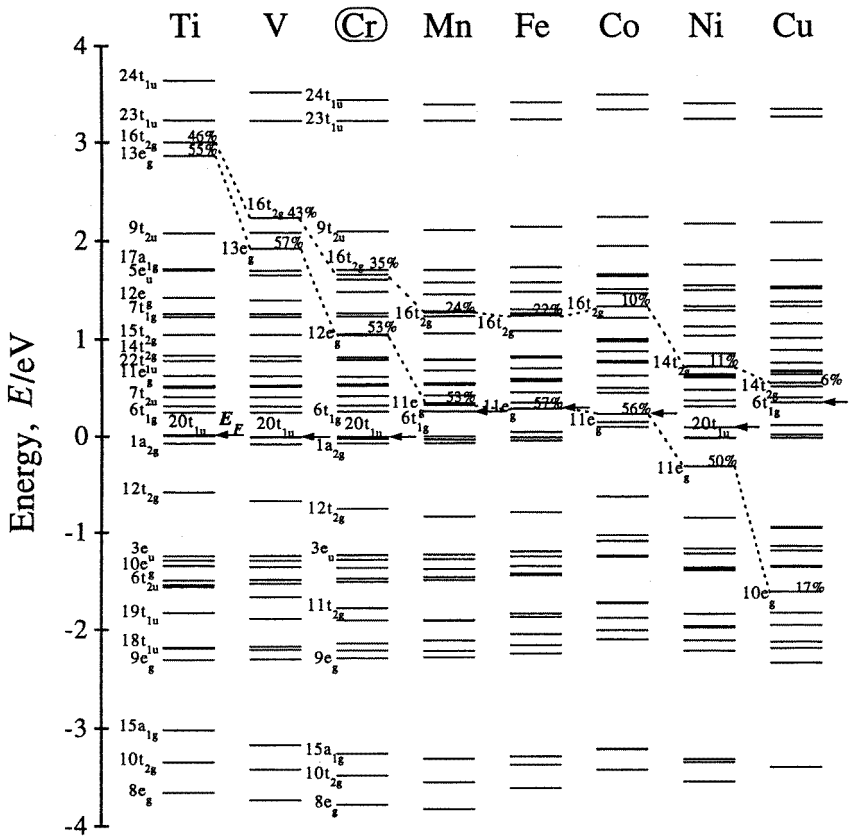

Figure 2. Energy level structures for pure Cr and alloyed Cr with 3d transition elements. The Fermi energy level of pure Cr is set to be 0 eV, and the Fermi energy level of alloyed Cr is indicated by an arrow.

attractive Coulomb interaction between the nucleus and d electrons which decreases with increasing average radius of d orbitals and hence with increasing atomic radius of the element. This leads to the appearance of the higher Md energy level for the larger element. However, this is not the case for Cu, Ag, Au, etc, in which the d orbitals are nearly fully occupied. In addition, the Md parameter was associated with the electronegativity [40] of alloying element M [40], except for Cu, Ag and Au, as shown in figures 3(a) and (b).

3.3. Electron density of states

The calculated electron density of states is shown in figure 4(a) for pure Cr. For comparison, the electron density of states for the central layer in a seven-layer Cr(001) film reported by Fu and Freeman [2] is shown in figure 4(b). This result was obtained using a full-potential linearized augmented-plane-wave (FLAPW) method. When figure 4(a) is compared with 4(b), it was seen that the positions of large peaks and valleys were similar even though there were some differences in the details. In figure 4(a), there were two characteristic large peaks near E_F in the partial density of states of d electrons. In other words, the Fermi level E_F was located near a large valley where there was a separation between the bonding and

Table 1. Fractions of the 3d, 4d and 5d components of alloying elements in the t_{2g} and the e_g orbitals.

		t_{2g}					e_g levels						
	M	$14t_{2g}$	$15t_{2g}$	$16t_{2g}$	$17t_{2g}$	$18t_{2g}$	$10e_g$	$11e_g$	$12e_g$	$13e_g$	$14e_g$	$15e_g$	$16e_g$
3d	Ti	0.7	0	46.1			1.0	0.3	0.7	55.1			
	V	1.1	0	43.0			1.5	0.7	5.0	57.4			
	Cr	2.1	0	34.8			2.2	4.0	53.1	5.5			
	Mn	4.4	0	23.8			3.3	52.8	4.6	0.7			
	Fe	5.6	0.3	21.8			3.7	56.6	2.6	0.6			
	Co	8.6	5.6	10.0			5.0	56.4	0.8	0.3			
	Ni	11.0	5.4	1.3			7.1	49.8	0.3	0.2			
	Cu	5.6	0.8	0.1			17.4	13.5	0	0			
4d	Zr		0.4	0.1	33.5			0.7	0.3	0.5	36.2		
	Nb		0.5	0	33.5			1.0	0.4	1.1	43.8		
	Mo		0.7	0	29.8			1.3	0.8	6.4	41.0		
	Tc		1.1	0	23.9			1.8	4.9	36.5	4.4		
	Ru		1.9	0	16.9			2.7	35.5	3.2	0.7		
	Rh		2.5	0.1	15.7			3.1	37.8	1.5	0.5		
	Pd		4.3	1.3	7.0			4.7	28.8	0.3	0.2		
	Ag		4.0	1.2	0.1			8.3	7.5	0	0		
5d	Hf			0.4	0	32.0				0.2	0.4	34.0	34.9
	Ta			0.5	0	31.8				0.3	0.9	40.6	23.9
	W			0.6	0	28.5				0.6	3.3	40.8	15.2
	Re			0.8	0	23.3				2.1	29.6	11.2	9.6
	Os			1.2	0	17.3				25.0	11.2	1.1	6.1
	Ir			1.5	0	14.9				31.9	2.4	0.5	5.2
	Pt			2.6	0.1	9.7				26.8	0.4	0.2	3.6
	Au			3.7	2.3	0.2				10.1	0.1	0.1	1.8

the antibonding energy region of d electrons. The d electrons occupied mainly the bonding orbitals, while leaving the antibonding orbitals unoccupied. This will yield an increasing stability of BCC Cr as was reported in other BCC metals such as Mo and W [34, 41]. In addition, it was apparent that the components of Cr 4s and 4p electrons extended to a wide energy range.

3.4. Bond order Bo

It is well known that the strength of the d–d covalent bonds contributes largely to the total cohesive energy of transition metals and alloys. Therefore, the bond order was calculated from the overlap populations of the d electrons between atoms in the cluster. Figure 5 shows the results, and their respective values are also given in table 2 together with the d-orbital energy level Md. In figure 5, for instance, M–$Cr^{(1)}$ refers to the bond order between the alloying element M and its first-nearest-neighbour $Cr^{(1)}$ atoms. Similarly, M–$Cr^{(2)}$ indicates the bond order between the alloying element M and its second-nearest-neighbour $Cr^{(2)}$ atoms. Also, $Cr^{(1)}$-$Cr^{(2)}$ indicates the bond order between the first- and the second-nearest-neighbour Cr atoms from a central alloying element M in the cluster. In the figure, the sum of these three bond orders is labelled Total. Both the $Cr^{(1)}$–$Cr^{(2)}$ and the M–$Cr^{(2)}$ bond orders scarcely changed with alloying elements, whereas the M–$Cr^{(1)}$ bond order varied largely with alloying elements. For example, the Ti addition to Cr made a

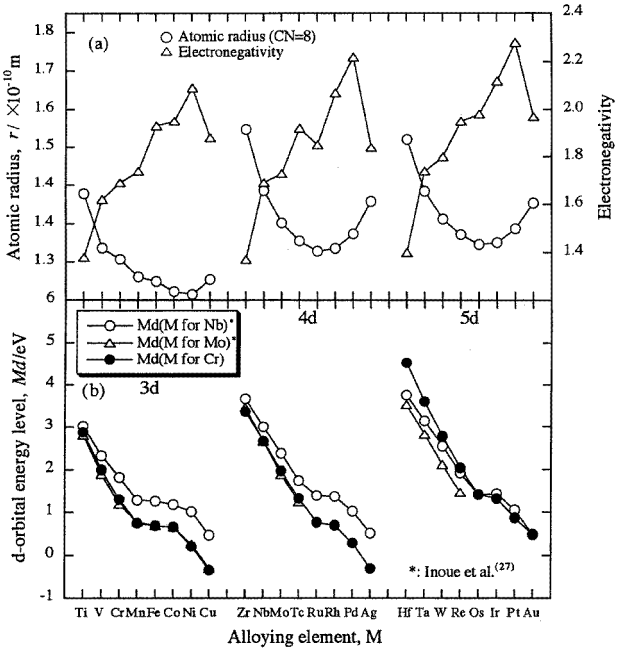

Figure 3. (a) Atomic radius (coordination number 8) and electronegativity of alloying elements, and (b) changes in the d-orbital energy level Md with alloying elements in Cr.

stronger chemical bond than did the Cu addition. Also, the total bond order was higher in the 4d and the 5d transition metals than in the 3d transition metals.

3.5. Ionicity

As shown in figure 6, the ionicity of each atom in the cluster was evaluated from the Mulliken [37] population analysis. In this figure, the ionicities of the $Cr^{(1)}$ atom and the $Cr^{(2)}$ atom are indicated by open triangles and open circles, respectively. In the figure, the results for pure Cr (M = Cr) are also shown for comparison. The ionicities were always positive for the second-nearest-neighbour $Cr^{(2)}$ atoms, but negative for the first-nearest-neighbour $Cr^{(1)}$ atoms, irrespective of the alloying elements in Cr. This ionicity difference between $Cr^{(1)}$ and $Cr^{(2)}$ atoms is simply due to the limited size of the cluster model employed in the present calculation. The ionicity of $Cr^{(2)}$ seemed to show little change with M. However, the ionicities of alloying elements indicated by full circles in the figure changed largely with the atomic number of elements. This change followed the variation in the electronegativity with the element M. For instance, Ti is most electropositive among the 3d series elements, and its ionicity was -0.038, whereas Ni is most electronegative and its ionicity was -0.406, a larger negative value than that for Ti.

3.6. Energy distribution of the overlap populations

The energy distributions of the overlap populations between d electrons are shown in figure 7(a) for Cr_{15}, in figure 7(b) for $FeCr_{14}$ and in figure 7(c) for $NiCr_{14}$ clusters. In this figure, each energy distribution curve was drawn by setting the Fermi energy level E_F

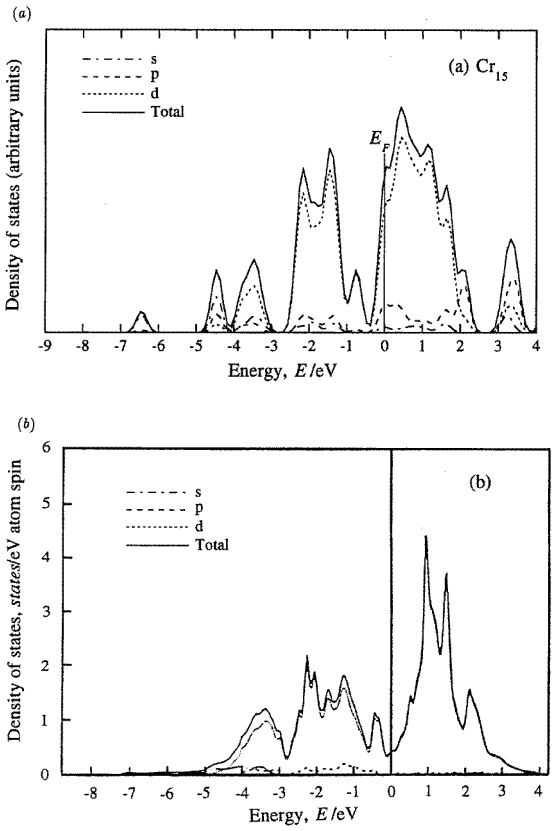

Figure 4. Electron density of states for (a) a Cr_{15} cluster and (b) a Cr (001) thin film [2].

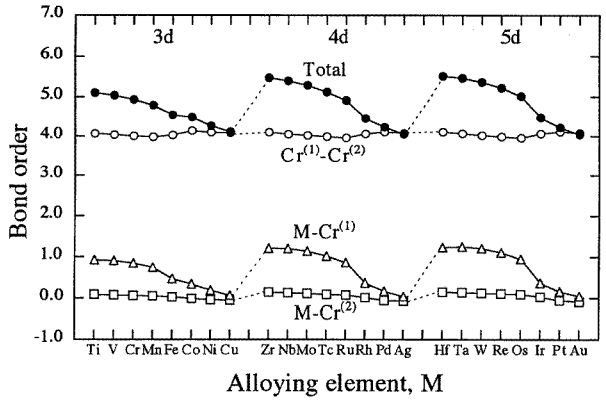

Figure 5. Changes in the bond order with alloying elements M in Cr.

to be zero. If the overlap population is positive (+), bonding-type interaction is operating between atoms whereas, if it is negative (−), antibonding-type interaction is dominant between atoms.

The Fermi energy level of the Cr_{15} cluster was located just at the position where the

Table 2. List of the bond order Bo and the d-orbital energy level Md for alloying elements in Cr.

Alloying element		Parameter	
	M	Bo	Md (eV)
3d	Ti	5.109	2.870
	V	5.041	1.998
	Cr	4.938	1.301
	Mn	4.801	0.752
	Fe	4.548	0.694
	Co	4.496	0.658
	Ni	4.276	0.213
	Cu	4.123	−0.346
4d	Zr	5.475	3.359
	Nb	5.403	2.662
	Mo	5.286	1.968
	Tc	5.125	1.324
	Ru	4.920	0.764
	Rh	4.457	0.697
	Pd	4.237	0.284
	Ag	4.059	−0.310
5d	Hf	5.517	4.518
	Ta	5.471	3.605
	W	5.368	2.768
	Re	5.221	2.037
	Os	5.022	1.422
	Ir	4.482	1.309
	Pt	4.233	0.875
	Au	4.050	0.496

overlap populations changed sign. In other words, the interaction changed from the bonding type to the antibonding type just at E_F. Thus, the d–d covalent interaction was found to be optimized in pure Cr, as explained earlier. On the other hand, the Fermi energy level of $FeCr_{14}$ and $NiCr_{14}$ was located at the energy region where the antibonding interaction was operating. Therefore, the d–d bond order became weaker in either $FeCr_{14}$ or $NiCr_{14}$ than in Cr_{15}, as shown in figure 5.

3.7. Electron density difference map

The spatial electron distribution in the cluster was examined using the electron density difference $\Delta\rho$. Here, $\Delta\rho$ was defined as

$$\Delta\rho = \rho(\mathrm{MCr}_{14}) - \rho(\mathrm{CrCr}_{14}) \tag{3}$$

where $\rho(\mathrm{MCr}_{14})$ and $\rho(\mathrm{CrCr}_{14})$ are electron densities of the clusters denoted in the parentheses. Therefore, $\Delta\rho$ means the change in the spatial electron distribution in the cluster with alloying. The calculated electron density difference maps on the (110) atomic plane are shown in figure 8(a) for M = V, in figure 8(b) for M = Mn and in figure 8(c) for M = Ni. In each figure, the region where $\Delta\rho > 0$ is indicated by full curves and the region where $\Delta\rho \leqslant 0$ is indicated by broken curves. Therefore, there is an electron excess in the region where $\Delta\rho > 0$, and electron deficiency in the region where $\Delta\rho \leqslant 0$. The

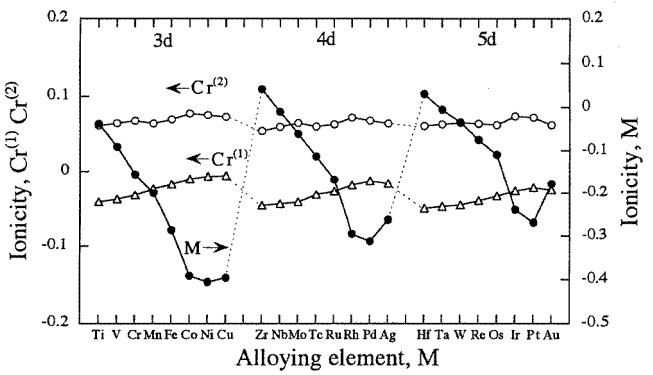

Figure 6. Ionicities of Cr and alloying elements, M, in Cr.

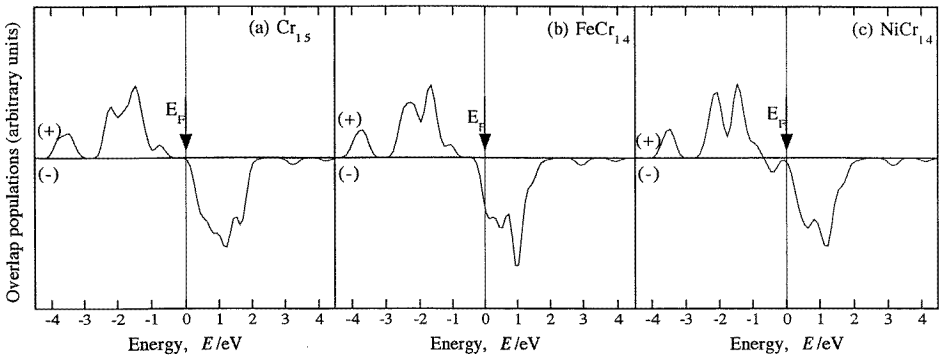

Figure 7. Changes in the overlap populations between d electrons for (a) Cr_{15}, (b) $FeCr_{14}$ and (c) $NiCr_{14}$.

appearance of a large positive or negative peak at the substitutional site is simply due to the difference between the total electron numbers of M and Cr atoms.

The changes in the bond orders with alloying elements shown in figure 5 could be understood from these electron density difference maps. For example, the differences between the electron densities of $Cr^{(1)}$ and $Cr^{(2)}$ atoms were almost zero regardless of alloying elements as indicated by A, B and C in figures 8(a)–(c), respectively. This was in agreement with little change in the $Cr^{(1)}$–$Cr^{(2)}$ bond order with alloying elements as shown in figure 5. Also, there was a slight increase in the electron density difference between a central V atom and the surrounding $Cr^{(1)}$ atom, as indicated by P in figure 8(a). In contrast with this, in the case of Mn substitution a negative electron density difference region was extended as indicated Q in figure 8(b). In the case of Ni substitution, a further negative electron density difference region was present in the region indicated R in figure 8(c). These results were consistent with the magnitudes of the V–Cr, Mn–Cr and Ni–Cr bond orders shown in figure 5.

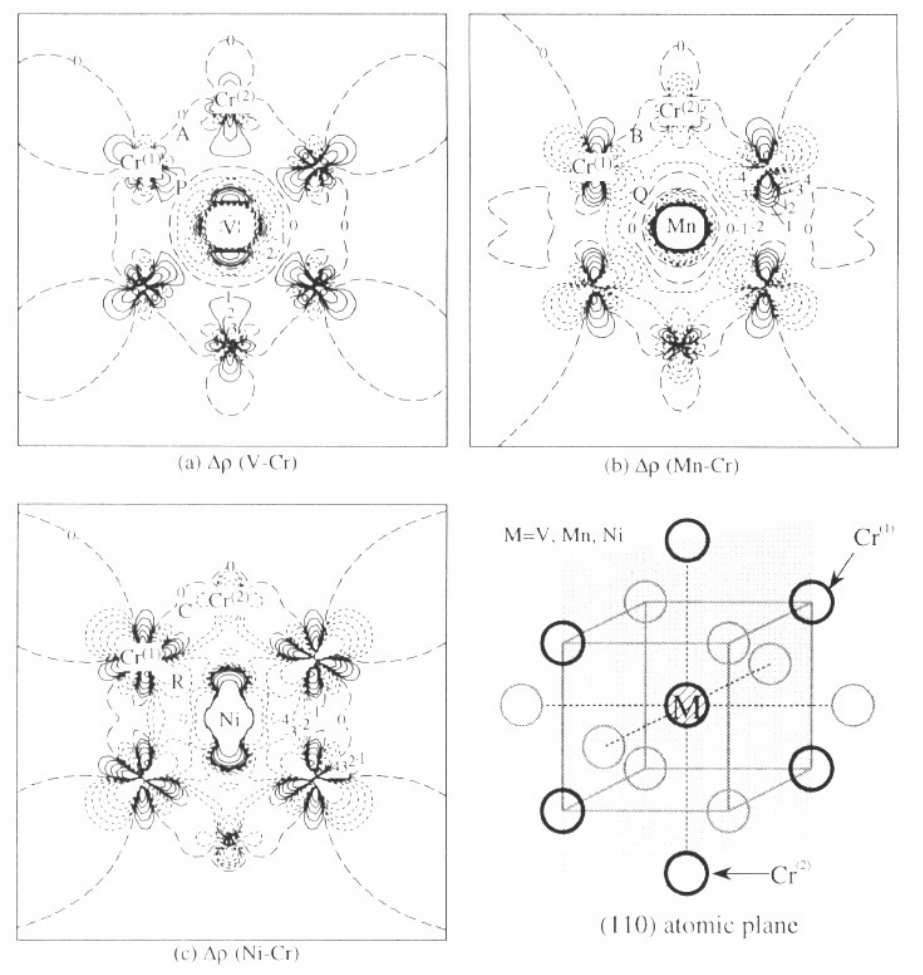

Figure 8. Electron density difference maps on the (110) atomic plane for (a) VCr_{14}, (b) $MnCr_{14}$ and (c) $NiCr_{14}$, where 0, ±1, ±2, ±3 and ±4 correspond to the electron density values 0, ±0.002, ±0.004, ±0.008 and ±0.016, respectively, in electrons per atomic unit cubed.

4. Discussion

4.1. Charge transfer and electronegativity

In order to understand the trend of charge transfer in alloyed Cr, the ionicity difference $I_M - I_{Cr^{(1)}}$ between the alloying element M and the surrounding $Cr^{(1)}$ atoms was calculated. The results are shown in figure 9, together with the electronegativity difference $\chi_M - \chi_{Cr}$ [40]. Here, the result for Cr denoted on the horizontal axis corresponds to the ionicity difference between a central Cr atom and the surrounding $Cr^{(1)}$ atoms in the pure Cr cluster.

Needless to say, the electronegativity is a measure of the charge transfer between atoms. Therefore, as might be expected, the ionicity difference was related closely to the electronegativity difference as shown in figure 9. In particular, a significant charge transfer took place in the direction from Cr to Co, Ni or Cu atoms. The amount of transferred charges in them seemed larger than expected from the electronegativity difference. Therefore, in

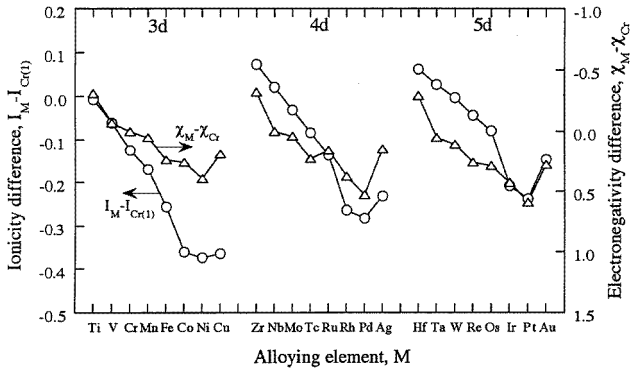

Figure 9. Ionicity difference between M and its first-nearest-neighbour chromium $Cr^{(1)}$ and electronegativity difference between M and Cr.

addition to the covalent interaction, the ionic interaction may be large in Cr alloys containing these elements.

4.2. Binary phase diagrams of Cr–M system

4.2.1. Solidus temperature. In our previous study, we have shown that there is a correlation between some thermal properties and the parameters obtained from the molecular orbital calculation. For example, the bond orders of pure BCC metals (e.g. Nb and Mo) are related to the heat of fusion [27]. The melting temperatures of pure metals also increase linearly with increasing bond order between atoms.

In this study, as shown in figure 10, the solidus temperatures of Cr–M binary alloys [42] were examined using the bond order Bo. Here, the solidus temperature means the lowest temperature above which the solid starts to melt. As is evident from this figure, the solidus temperature of Cr–6.7 mol%M and Cr–11.1 mol%M alloys increased monotonically with increasing calculated bond order except for Ti.

Furthermore, creep resistance is one of the most important properties for the design of high-temperature materials such as Cr alloys. It is known that the creep phenomenon often takes place by the atomic diffusion mechanism. As the activation energy for atomic diffusion in solids is generally proportional to the melting temperature, the bond order will be indeed give a good indication to show the creep resistance of the Cr alloys. The addition of high-Bo elements will enhance the creep resistance of alloys.

4.2.2. Intermetallic compounds. Both the d-orbital energy level Md and the bond order Bo are convenient parameters for describing the phase constitution in alloys [43]. This is because these parameters Md and Bo are associated with the nature of the chemical bond between atoms in solids. In this study, these two parameters were also employed in order to explain the appearance of the intermetallic compounds in Cr alloys, assuming that the general trend of the chemical bond between M and Cr atoms in BCC Cr still holds even in Cr-rich intermetallic compounds. The location of each alloying element on the Bo versus Md map (hereafter called the Bo–Md map) is shown in figure 11. In the figure, intermetallic compounds existing on the Cr-rich side of binary phase diagrams [42, 44] are indicated using different symbols. There are six types of intermetallic compound in binary Cr alloys; Laves phase (C15), σ-phase ($D8_b$), AB_3 (A15), AB ($L1_0$), AB_2 and AB_4 ($D1_a$).

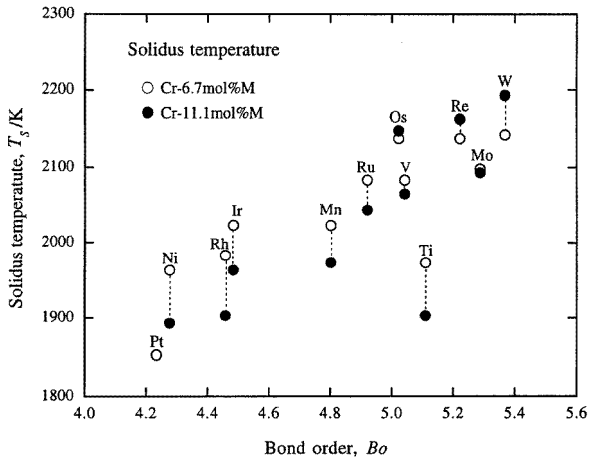

Figure 10. Correlation of the solidus temperatures of Cr–6.7 mol%M and Cr–11.1 mol%M alloys with the bond order *Bo* for M.

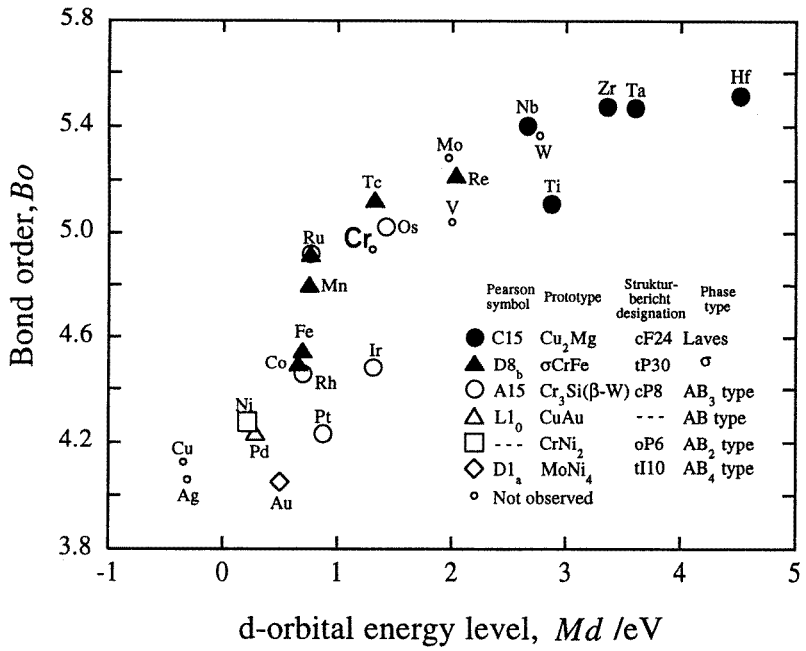

Figure 11. Location of alloying elements on the *Bo–Md* map and types of intermetallic compound in binary Cr alloys.

It is interesting to note that the same types of compound are located in a certain small region on the *Bo–Md* map. For example, the elements of Hf, Ta, Zr, Nb and Ti, all of which have high *Bo* and high *Md* values, produces the Cu_2Mg-type Laves phase. The second group of elements, Re, Tc, Ru, Mn, Fe and Co, which have high *Bo* and middle *Md* values, makes the complex σ-phase. Also, the third group of elements, Ru, Os, Rh, Ir and Pt, makes the intermetallic compounds of the AB_3 type and it was located approximately near the pure Cr

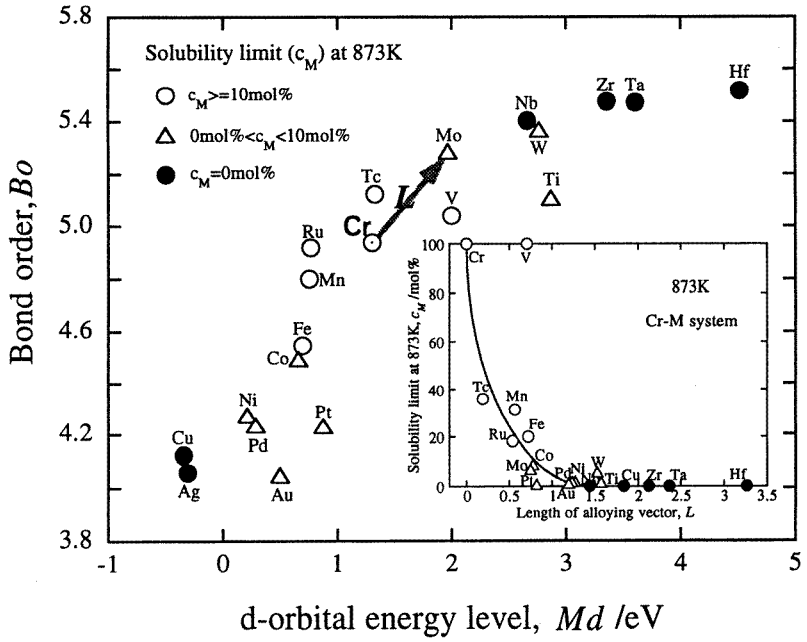

Figure 12. Solubility limit presented on the Bo–Md map and its correlation with the length L of the alloying vector for various Cr–M systems.

position on the map. On the other hand, some ordered phases of AB ($L1_0$), AB_2 and AB_4 ($D1_a$) types appeared in the alloys containing those elements which have low Bo and low Md values. From these results, it was apparent that the types of intermetallic compound which are in equilibrium with the Cr-rich terminal solid solution will be predictable with the aid of the Bo and Md parameters.

4.2.3. Solubility limit. The solubility limit of alloying elements in a terminal solid solution is one of the important factors when we treat the phase stability problem of alloys. Therefore, it has been estimated by employing various parameters, e.g. the electronegativity and the atomic radius [45, 46]. Recently, Morinaga *et al* [29, 30] have shown that the solid solubility in the transition-metal-based FCC alloys is described well by the d-orbital energy level Md. They have also shown in the case of BCC alloys that the solubilities are dependent not only on the Md parameter but also on the Bo parameter. So, in this study, the solubility limits of BCC Cr alloys were estimated using the Md and Bo parameters. The results are shown in figure 12.

The solubility limits of M decreased with increasing distance between the M and the Cr positions on the map. So, an alloying vector for each M was defined by a line connecting the M position with the Cr position on the Bo–Md map. For example, the case of M = Mo is shown in the figure. The length L of the alloying vector was then given by

$$L = [(Md_M - Md_{Cr})^2 + (Bo_M - Bo_{Cr})^2]^{1/2}. \tag{4}$$

Here, Md_M and Bo_M are the Md and the Bo parameters for the alloying element M, respectively, and Md_{Cr} and Bo_{Cr} are the corresponding parameters for Cr (i.e. M = Cr). The solubility limit at 873 K in the Cr solid solution was well represented by the length L

of this alloying vector as shown as an inset in figure 12. The solubility limit c_M at 873 K was small (0 mol% $< c_M <$ 10 mol%) when L exceeded 0.8, and zero when L exceeded 1.8. Apparently, it decreased monotonically with increasing L. In this sense, the present approach will provide us with a tool for evaluating the phase stabilities of Cr alloys.

5. Conclusions

The electronic structures of Cr-containing alloying transition elements were investigated by the DV–Xα cluster method. The nature of chemical bonds between alloying elements and Cr atoms was clarified from a series of analyses of the electronic structures. The two alloying parameters, the d-orbital energy level and the bond orders, were determined for various elements in Cr. These parameters correlated with the solidus temperatures and solid solubility limits of binary Cr alloys. It was also shown that the types of intermetallic compound in binary alloys could be classified using these two parameters. It was concluded that the molecular orbital approach was very useful in describing the alloying behaviour of BCC Cr.

Acknowledgments

The authors would like to acknowledge the staff of Computer Center of the Institute for Molecular Science at Okazaki National Institutes for the use of the NEC SX-3 model 34R supercomputer. This research was supported in part by the Grant-in-Aid for Scientific Research from the Ministry of Education, Science and Culture of Japan.

References

[1] Ohba Y 1972 *Bull. Jpn. Inst. Met.* **11** 105
[2] Fu C L and Freeman A J 1986 *Phys. Rev.* B **33** 1755
[3] Fawcett E 1988 *Rev. Mod. Phys.* **60** 209
[4] Kosugi M, Tso N C and Sanchez J M 1989 *Solid State Ion. Diffus. React.* **32–33** 714
[5] Leiro J A and Minni E E 1984 *Phil. Mag.* B **49** 61
[6] Sugawara H, Naito K, Miya T, Kakizaki A, Nagakura I and Ishii T 1984 *J. Phys. Soc. Japan* **53** 279
[7] Pattnaik P C, Dickinson P H and Fry J L 1983 *Phys. Rev.* B **28** 5281
[8] Fischer D W 1971 *Phys. Rev.* B **4** 1778
[9] Wain H L, Henderson F and Johnstone S T M 1954–5 *J. Inst. Met.* **83** 133
[10] Wain H L, Henderson F, Johnstone S T M and Louat N 1957–8 *J. Inst. Met.* **86** 281
[11] Abrahamson E P and Grant N J 1958 *Trans. Am. Soc. Met.* **50** 705
[12] Maykuth D J, Klopp W D, Jaffee R I and Goodwin H B 1955 *J. Electrochem. Soc.* **102** 316
[13] Allen B C and Jaffee R I 1963 *Trans. Am. Soc. Met.* **56** 387
[14] Allen B C, Maykuth D J and Jaffee R I 1963 *Trans. Metall. Soc. AIME* **227** 724
[15] Sigli C and Sanchez J M 1988 *Acta. Metall.* **36** 367
[16] Kotani A 1974 *J. Phys. Soc. Japan* **36** 103
[17] Mattheiss L F and Hamann D R 1986 *Phys. Rev.* B **33** 823
[18] Ishikawa A 1982 *J. Phys. Soc. Japan* **51** 441
[19] Laurent D G, Callaway J, Fry J L and Brener N E 1981 *Phys. Rev.* B **23** 4977
[20] Fry J L, Brener N E, Laurent D G and Callaway J 1981 *J. Appl. Phys.* **52** 2101
[21] Fry J L, Brener N E, Thompson J L and Dickinson P H 1980 *Phys. Rev.* B **21** 384
[22] Bakenev V L, Lisenko A A and Zhurakovskii E A 1985 *Izv. VUZ Fiz.* **28** 72
[23] Morinaga M, Yukawa N and Adachi H 1986 *Tetsu-to-Hagané* **72** 555
[24] Morinaga M, Yukawa N and Adachi H 1985 *J. Phys. F: Met. Phys.* **15** 1071
[25] Morinaga M, Yukawa N and Adachi H 1988 *Bull. Japan Inst. Met.* **27** 165
[26] Morinaga M, Murata Y and Ezaki H 1992 *Proc. Int. Symp. on Materials Chemistry in a Nuclear Environment (Tsukuba, 1992)* p 241

[27] Inoue S, Saito J, Morinaga M and Kano S 1994 *J. Phys.: Condens. Matter* **6** 5081
[28] Morinaga M, Yukawa N and Adachi H 1985 *Tetsu-to-Hagané* **71** 1441
[29] Morinaga M, Yukawa N, Ezaki H and Adachi H 1985 *Phil. Mag.* A **51** 223
[30] Morinaga M, Yukawa N, Ezaki H and Adachi H 1985 *Phil. Mag.* A **51** 247
[31] Slater J C 1979 *The Calculation of Molecular Orbitals* (New York: Wiley)
[32] Averill F W and Ellis D E 1973 *J. Chem. Phys.* **59** 6413
[33] Adachi H, Tsukada M and Satoko C 1978 *J. Phys. Soc. Japan* **45** 875
[34] Adachi H and Imoto S 1978 *Bull. Japan Inst. Met.* **17** 490, 495
[35] Ellis D E and Painter G S 1970 *Phys. Rev.* B **2** 2887
[36] Yang C Y, Johnson K H, Salahub D R, Kaspar J and Messmer R P 1981 *Phys. Rev.* B **24** 5673
[37] Mulliken R S 1955 *J. Chem. Phys.* **23** 1833, 1841, 2339, 2343
[38] Satoko C, Tsukada M and Adachi H 1978 *J. Phys. Soc. Japan* **45** 1333
[39] Teatum E T, Gshneidner K A Jr and Waber J T 1968 *Department of Commerce, Washington, DC, USA, Report* LA-2345
[40] Watson R E and Bennett L H 1978 *Phys. Rev.* B **18** 6439
[41] Miyazaki E (ed) 1991 *Fundamentals and Applications of Surface Science* (Tokyo: NTS)
[42] Massalski T B (ed) 1990 *Binary Phase Diagrams* vol 1–3, 2nd edn (Metals Park, OH: American Society of Metals)
[43] Morinaga M, Yukawa N, Maya T, Sone K and Adachi H 1988 *Proc. 6th World Conf. on Titanium* (Paris: Société Française de Métallurgie) p 1601
[44] Japan Institute of Metals 1990 *Metals Data Book* (Tokyo: Maruzen) p 55
[45] Hume-Rothery W and Raynor G V 1954 *Structures of Metals and Alloys* (London: Institute of Metals)
[46] Darken L and Gurry R W 1953 *Physical Chemistry of Metals* (New York: McGraw-Hill)